Influence of the pressure field distribution in Transcranial ultrasonic neurostimulation

Youliana Younan, Thomas Deffieux, Benoit Larrat, Mathias Fink, Mickael Tanter, Jean-Francois Aubry

Influence of the pressure field distribution in Transcranial ultrasonic neurostimulation

Youliana Younan, Thomas Deffieux, Benoit Larrat, Mathias Fink, Mickael Tanter, Jean-Francois Aubry

Institut Langevin, ESPCI-ParisTech, CNRS UMR7587, INSERM U979,
1 rue Jussieu, Paris, France

Abstract

Purpose

Low-intensity focused ultrasound has been shown to stimulate the brain non-invasively and without noticeable tissue damage. Such a non-invasive and localized neurostimulation is expected to have a major impact in neuroscience in the coming years. This emerging field will require many animal experiments to fully understand the link between ultrasound and stimulation. The primary goal of this paper is to investigate transcranial ultrasonic neurostimulation at low frequency (320 kHz) on anesthetized rats for different acoustic pressures and estimate the *in situ* pressure field distribution and the corresponding motor threshold, if any. The corresponding acoustic pressure distribution inside the brain, which cannot be measured *in vivo*, is investigated based on numerical simulations of the ultrasound propagation inside the head cavity, reproducing at best the experiments conducted in the first part, both in terms of transducer and head geometry and in terms of acoustic parameters.

Methods

In this study, 37 ultrasonic neurostimulation sessions were achieved in rats (N=8) using a 320 kHz transducer. The corresponding beam profile in the entire head was simulated in order to investigate the *in situ* pressure and intensity level as well as the spatial pressure distribution, thanks to a rat micro-computed tomography scan (CT)-based 3D finite differences time domain solver.

Results

Ultrasound pulse evoked a motor response in more than 60% of the experimental sessions. In those sessions, the stimulation was always present, repeatable with a pressure threshold under which no motor response occurred. This average acoustic pressure threshold was found to be 0.68 ± 0.1 MPa (corresponding mechanical index, MI =1.2 and spatial peak, pulse averaged intensity, Isppa = 7.5 $W.cm^{-2}$), as calibrated in free water. A slight variation was observed between deep anesthesia stage (0.77 ± 0.04 MPa) and light anesthesia stage (0.61 ± 0.03 MPa), assessed from the pedal reflex. Several kinds of motor responses were observed: movements of the tail, the hind legs, the forelimbs, the eye and even a single whisker were induced separately. Numerical simulations of an equivalent experiment with identical acoustic parameters showed that the acoustic field was spread over the whole rat brain with the presence of several secondary pressure peaks. Due to reverberations, a 1.8-fold increase of the spatial peak, temporal peak acoustic pressure (Psptp) (± .4 standard deviation), a 3.6-fold increase (± 1.8) for the spatial peak, temporal peak acoustic intensity (Isptp), and 2.3 for the spatial

peak, pulse averaged acoustic intensity (Isppa), were found compared to simulations of the beam in free water. Applying such corrections due to reverberations on the experimental results would yield a higher estimation for the average acoustic pressure threshold for motor neurostimulation at 320 KHz at 1.2± 0.3 MPa (MI=2.2±0.5 and Isppa=17.5 ± 7.5 $W.cm^{-2}$).

Conclusions

Transcranial ultrasonic stimulation is pressure- and anesthesia-dependent in the rat model. Numerical simulations have shown that the acoustic pattern can be complex inside the rat head and that special care must be taken for small animal studies relating acoustic parameters to neurostimulation effects, especially at a low frequency.

1. Introduction:

Ultrasound is known to have multiple interactions with living tissues. While most of the time those effects have been studied to ensure that imaging techniques remain safe with as little interaction as possible with tissues, they can also be used for therapeutic purposes. Therapeutic ultrasound relies mainly on two specific interactions of ultrasound with tissues: thermal and mechanical effects. The former can be used to thermally ablate the tissue due to the absorption of a high intensity focused ultrasound beam[1], while the latter is involved in kidney stone comminution (lithotripsy), which is the most widespread application of therapeutic ultrasound[2]. However, more subtle and reversible effects can be induced with ultrasound.

In 1958, Fry[3] was able to demonstrate that the transmission of ultrasound waves to the lateral *geniculate nucleus* could suppress the induced response in the primary visual cortex in cats, as evidenced by standard electroencephalogram recordings (EEG). In 1976, Gavrilov and colleagues[4] studied the effect of ultrasound in humans and demonstrated that it was a powerful tool to stimulate nerve structures and produce different thermal, tactile, and pain responses. Later, Tyler and colleagues[5, 6], proved the ability of low frequency, low intensity ultrasound waves in inducing motor stimulation without producing damages to the brain tissue. Yoo and colleagues[7] obtained similar results in rabbits in 2010 and used a magnetic resonance imaging (MRI)-compatible transducer to visualize the activation of the motor cortex using functional MRI.

Using multi-element transducers and phase correction, ultrasound can be focused through the intact human skull[8–10], making it possible to translate these animal studies to humans.

Compared to current non-ultrasonic neurostimulation techniques such as transcranial direct current stimulation (tDCS)[11], implanted electrodes[12], Transcranial Magnetic Stimulation (TMS)[13] or optogenetics[14, 15], transcranial ultrasonic neurostimulation offers a unique combination of high spatial resolution (a few millimeter), good time resolution (few hundreds of milliseconds), good access to deep brain structures and non-invasiveness. Transcranial ultrasound neurostimulation could thus open the door to unique high resolution and non-invasive neurostimulation applications. Recent results confirm this potential, as focused ultrasound was able to modulate the level of cortical neurotransmitters[16] and thus, may have diagnostic as well as therapeutic implications for DA/5-HT-mediated neurological and psychiatric disorders.

There remain important questions on the mechanisms behind ultrasound neurostimulation. On the physiological scale, different hypotheses have been proposed

from the ultrasound-induced release of neurotransmitters inside the synaptic cleft[17] to the ultrasound-induced opening of mechano-sensitive channels on the membrane[18] that would then trigger action potentials[5]. On a more macroscopic scale, it has not yet been demonstrated if the effect is linked to thermal or mechanical interactions of the ultrasound beam with neuronal tissue, which is nonetheless critical to optimize efficacy and safety. One way to investigate those interactions is to vary ultrasound parameters such as pressure, burst length and frequency and to study the resulting stimulation strength. However, in that case, the existence of an acoustic threshold lower bound for the effect was even raised, as Tyler et al. interestingly reported higher electromyography (EMG) responses when lower acoustic intensities were used[6]. On the contrary, King et al.[19] reported an acoustic threshold below which no stimulation was observed for ultrasonic neurostimulation in rats.

In order to further investigate the potential mechanisms involved, the exact value of the *in situ* acoustic threshold in the brain need to be extrapolated, as well as the spatial distribution of the beam (for correlation with brain structures), due to the presence of standing waves. While investigating ultrasonic blood brain barrier opening, O'Reilly et al.[20] reported pressure modulation due to standing waves, as measured in a rat skull inside a water tank. We propose here to take advantage of numerical simulations to investigate the spatiotemporal pressure field using a full rat head model surrounded by air, in the same experimental conditions used for neurostimulation.

In this paper, we first studied the motor response of 8 rats using a low frequency transducer (320 KHz) transcranially for different ultrasonic pressure levels. We investigated the different kinds of elicited motor responses and the existence of an acoustic pressure threshold for the response. Since the exact pressure in the head cavity cannot be measured *in vivo*, the corresponding acoustic field was then simulated numerically using a full rat head 3D computed tomography (CT) scan and finite-difference time-domain (FDTD) software with identical acoustic parameters. The simulated pressure peak and spatial distribution inside the head cavity were then compared to that which was simulated in water. The correction of the motor thresholds for *in situ* pressure and the acoustic field spatial distribution are then discussed.

2. Materials and Methods:

2.1 Experimental setup

A custom holder was used to lift the body of the animal while allowing free motion of its tail, forelegs and hind legs in order to easily visualize motor excitations. A stereotactic frame (502603, WPI, Sarasota, FL,USA) was used to immobilize the head. A single element focused ultrasound transducer (H115, Sonic Concepts, Bothell, MA, USA) (central frequency 250 KHz, diameter 64 mm, FD# 1) was used. A coupling cone (C103, Sonic Concepts, Bothell, WA, USA) filled with degassed water was used in between the transducer and the animal head (Figure 1). The transducer was fixed on two linear motors (Micos sMc Pollux, Freiburg, Germany) that allow a translation inside the horizontal plane to position the transducer over the desired target area. Echographic gel (Aquasonic 100, Parker Laboratories Inc., Fairfield, NJ, USA) was applied between the head to ensure acoustic coupling. All experiments were recorded on video to allow further determination of the motor threshold. The motor response was then manually classified in three categories: no response, moderate or strong motor response. A strong motor response was considered when a clear limb movement was elicited. Moderate

motor response was considered when a muscular contraction was clearly visible but no limb movement occurred. Visual motor response classification was preferred to electromyography recordings (EMG) because EMG measurements were found to be affected by electrical cross-talk with the transducer driving signals. Several electrodes and shielding have been tested but too many false responses were recorded, as demonstrated by additional measurements without coupling gel and thus without actual ultrasound transmission.

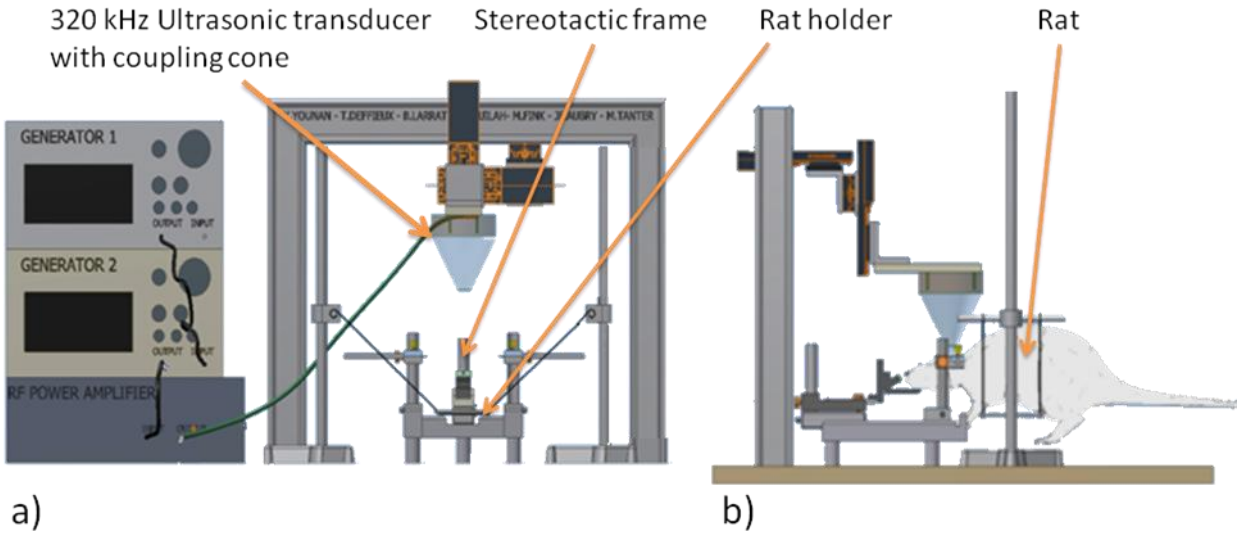

Figure 1 (a, b): a - Experimental setup showing the stereotactic frame, ultrasound transducer, linear motors and support frame with the electronics equipment, b - Schematic diagram with the animal positioned in the stereotactic frame and holder. The transducer with coupling cone is positioned on the head of the animal.

2.2 Ultrasound sequence and calibration

The ultrasound sequence used is based on the protocol of Tufail et al.[21], with a slightly higher center frequency of 320 kHz instead of 300 kHz; this corresponds to a peak in the transducer spectrum and a longer total sonication duration of 250 ms instead of 100ms, which was found to be more efficient.

The detailed parameters are as follows: ultrasound frequency was 320 KHz, number of cycles was 75 per pulse (pulse duration = 230 µs), pulse repetition frequency (PRF) was 2 KHz (duty-cycle=50%) and the total burst duration was 250 ms. Only the pressure was changed in this study to identify the threshold, and ranged from 0.4 MPa to 1 MPa.

In order to build such sequence, two generators were used (AFG3101, Tektronix, Melrose, MA); a 75 Watt amplifier (75A250A, Amplifier Research, Souderton, PA) was then used to deliver the required power to the transducer and the input voltage of the transducer was monitored using an oscilloscope (TDS2022B, Tektronix, Melrose, MA) and voltage probe (P6139A, Tektronix, Melrose, MA).

The transducer was calibrated with a custom built heterodyne interferometer[22] in degassed water. The heterodyne interferometer uses a laser beam to detect the small

vibration of the ultrasound wave on a mylar membrane which is then converted to pressure.

The calibration was first performed in free water. It was also performed behind three excised rat skulls. The skulls were cut in half in the horizontal plane to allow the positioning of the mylar membrane just behind the top of the skulls. Transmission through the rat skulls was measured at three different locations for all skulls, as shown in figure 2: position A at +1, +1 mm from Lambda (N=3 skulls), position B at -1.5, -1.5 mm from Bregma (N=3 skulls) and position C at Bregma (N=1 skull).

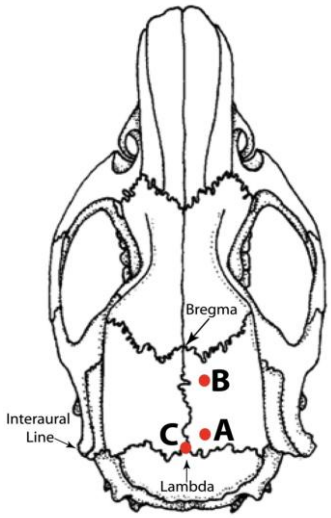

Figure 2: Location of the transmission measurements locations through the rat skulls

2.3 Animal preparation and ultrasound neurostimulation protocol

All animals were Sprague Dawley rats (N=8; all male, body weight 150-250 g). Each rat was shaved prior to the experiment and was injected intraperitoneally with Ketamine and Xylazine for sedation (66 mg Ketamine for 1 kg body weight, 13 mg Xylazine for 1 kg body weight). Eight to ten minutes after anesthesia, and once the rat was deeply anesthetized, the animal was placed on the holder and his head was fixed in the stereotactic frame. A coupling gel was placed over the rat head and the ultrasonic transducer was positioned using the motors at the desired location.

25 to 30 minutes after injection, we started to apply ultrasound pulses every 10 seconds to the rat brain with a pressure of 0.75 MPa, as estimated from the calibration measured in free water, around the locations Lambda –1 mm, - 1 mm and -3 mm as can be seen in Figure 2. These chosen locations correspond to the best success rate in obtaining motor responses, even though they did not correspond to the motor cortex area. The position was adjusted during this phase to find the best motor responses, although it was generally stable when moved less than a few millimeters. When a stable response was obtained, the pressure was reduced until the response was barely noticeable.

For each series of measurements, 30 different pressure amplitudes centered around this value were defined randomly in order to investigate the motor responses versus pressure curves. New series were added until the rat started to wake up and to show

motor activity uncorrelated with the ultrasound pulses. This temporal window of acceptable anesthesia level typically lasted around 10 to 15 minutes depending on the rat weight and anesthesia strength. Meanwhile, the anesthesia level was regularly estimated by assessing the pedal reflex of the rat, considering that no reflex meant a deep anesthesia level and a reflex meant a lower anesthesia level. For each series, experimental points were fitted with a sigmoid using Matlab (MathWorks, Natick, MA, USA) in order to obtain a more accurate threshold value for the motor response.

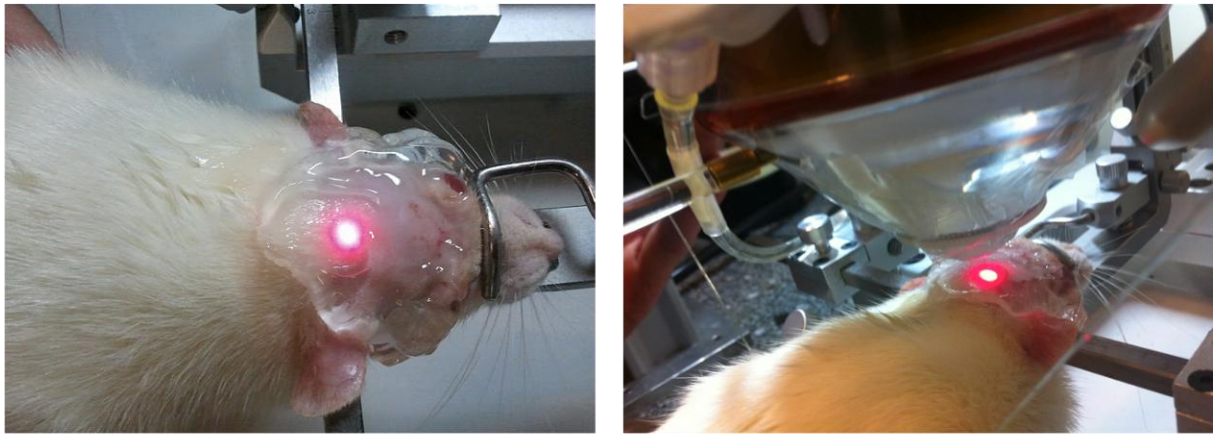

Figure 3 (a, b): The ultrasound transducer is initially positioned close to the lambda anatomical point and has been marked by a laser beam here. The rat head is shaved and echographic gel was inserted between the coupling cone and the rat skin.

Possible damage was investigated by careful examination of the skin of the rats after the experiment and one day later. The behavior of the rats was also investigated over several days after each neurostimulation session and their weight controlled. No change in behavior or weight was observed, although no histology was performed in this study. In order to minimize the number of animals required for the study, each rat underwent several neurostimulation sessions with at least one week of recovery between each.

2.4 Numerical simulation of the experimental setup

In order to investigate the ultrasound field in the whole rat brain while taking into account complex effects of the full skull cavity and head geometry, three-dimensional (3D) numerical simulations of the ultrasound propagation were conducted. Acoustic density and velocity maps were reconstructed from a 80 µm micro-CT scan (Skyscan1178, Bruker micro-CT, source 65kV) of a rat head using an approach validated on different animal models[23–26]. The skull was considered as a homogeneous layer since the only apparent variations were due to the smoothing from the CT reconstruction algorithm and not to the microstructure. The acoustic parameters are summarized in table 1. The acoustic density and velocity 3D maps were then sub-sampled to a 240 µm isotropic resolution which gave a ratio of 20 pixels per wavelength.

An in-house 3D finite-difference time-domain acoustic simulation software (Acel, Institut Langevin, Paris, France), was used to perform the purely acoustic and linear ultrasound propagation simulation through skull structures[23–25]. The coupling cone and

the tissue-air interfaces around the head were modeled as perfectly reflecting interfaces since the reflection coefficients between water and air and between tissue and air are close to 99.9% (Z_{air}=408 Pa.s/m, Z_{water}=Z_{tissue}=1.5 .10^6 Pa.s/m).

	Water	Brain	Skull	Other tissue
Velocity(m/s)	1540	1560[27]	3000[25]	1540
Density (kg/m^3)	1000	1040[27]	1850[25]	1000
Attenuation (dB/cm)	0	0.6 @ 1 MHz[27]	6.9 @ 1 MHz[28]	0.3 @ 1 MHz
		0.19 @ 320 kHz	2.2 @ 320 kHz	0.1 @ 320 kHz

Table 1: Acoustic parameters used in the rat head model

Three simulations were performed: one in free water, one behind the half-skull immersed water and one inside the full head cavity in air. The same acoustic parameters were used as in the experimental setup but the total simulation duration was limited to 500 µs of which 230 µs corresponded to a single ultrasonic pulse, as defined in the "ultrasound calibration and sequence" subsection (i.e. the full 75 periods of the 320 kHz ultrasound burst).

For each simulation, the pressure field was stored in three dimensions for all time steps in a 180 gigabyte file.

Time profiles of the acoustic pressure were extracted at the geometric focus for the three configurations and normalized to the spatial peak, time peak pressure simulated in free water. The spatial peak position in free water corresponds to the acoustic focus of the transducer which is slightly closer to the transducer than the geometric focus at low frequencies.

Maps of the *in situ* time peak pressure were also estimated by taking the time peak of the pressure field at each pixel for the sagittal, coronal and horizontal views, centered on the geometric focus. All maps were then normalized to the spatial peak, time peak pressure simulated in free water.

Spatial peak, time peak pressures (Psptp) were estimated for each configuration to discuss the effect of reverberations. Those values were normalized to the Psptp simulated in water.

Spatial peak, time peak acoustic intensities (Isptp) were estimated for each configuration by squaring the Psptp with the same normalization.

Spatial peak, pulse averaged acoustic intensities (Isppa) were estimated for each configuration by first squaring the space-time pressure field then averaging over the 75 cycles (taking into account the propagation delay for each pixel) and finally taking the spatial maximum. Those values were normalized to the Isppa simulated in free water.

For the estimations of these normalized values, only the acoustic field inside the brain volume was taken into account, disregarding any other peaks outside of this volume.

In order to investigate the robustness of those results with respect to the transducer position, 10 different locations of the transducer were simulated. These locations were chosen randomly in a cube of length equal to the wavelength (i.e. 5 mm at 320 kHz) to generate different configurations of interference patterns between the transducer and the skull surface. This artificially increases the standard deviation of the estimated values but provides more insight on the influence of the transducer-skull interferences with respect to the intra head cavity reverberations.

3. Results

3.1 Ultrasound pressure calibration through the half skulls

Measurements of the ultrasound transmission through the rat half-skulls shows that, on average, for the three positions tested, 89% of the pressure amplitude can be recovered behind the half-skulls immersed in water (see table 2). This is to be expected due to the low frequency used here (320 kHz) as skull thicknesses were estimated to be approximately 0.41 mm +/-0.16 mm using a digital caliper rule (Fischer Darex, Le Chambon Feugerolles, France).

In specific cases, transmission could be higher than 100%, which is due to the constructive interferences between the skull sample and the transducer surface and can also be observed in simulations with the half skull model.

Transmission	Position A	Position B	Position C	All measurements
320 KHz	91±8%	83±9%	75% (std N/A)	89±10%

Table 2: Transcranial transmission coefficient over the three different points on the skulls surface. Positions tested are given in the Method section.

3.2 Ultrasound neurostimulation experiments

Following the protocol described in the Material & Methods section, we routinely obtained motor responses of the tail and hindlegs in more than 60% of the experimental sessions. In the case of failed experiments (40%), no stimulation at all could be observed for any of the trials performed on a given day for a given animal and for any acoustic pressure tested (up to 1 MPa). Successful experiments, however, were consistent and always repeatable during the same day. They were strong and clearly visible to the naked eye.

In those cases, a reproducible response was observed above a pressure threshold. Figure 4(a, b, c) illustrates such motor response obtained in a rat with a strong tail movement triggered by the ultrasound pulse.

While the observed motor responses largely involved the hindlegs and the tail, other motor responses have also been observed, such as contraction of the forelimbs or facial muscles, without tail or hindleg movement. These other motor responses did not seem to be linked to a particular position of the ultrasound transducer on the skull but were perfectly reproducible during the whole experimental session duration.

In some experimental sessions (N=3), we were also able to trigger a motor response of the occulomotor system alone (cf. figure 4(d, e, f)) yielding a movement of the eyes. Both eyes were seen to move in the same direction. The focus zone was approximately 3 mm anterior, –2 mm right to the lambda point and the effects remained visible a few millimeters around this point.

In another experimental session (N=1), we were able to trigger the motor response of a single whisker (cf. figure 4(g, h, i)) during the whole duration of the experiment. Only the left whisker was seen to move. The focus point was contralateral to the whisker movement, 3 mm anterior, –1 mm right to the lambda point.

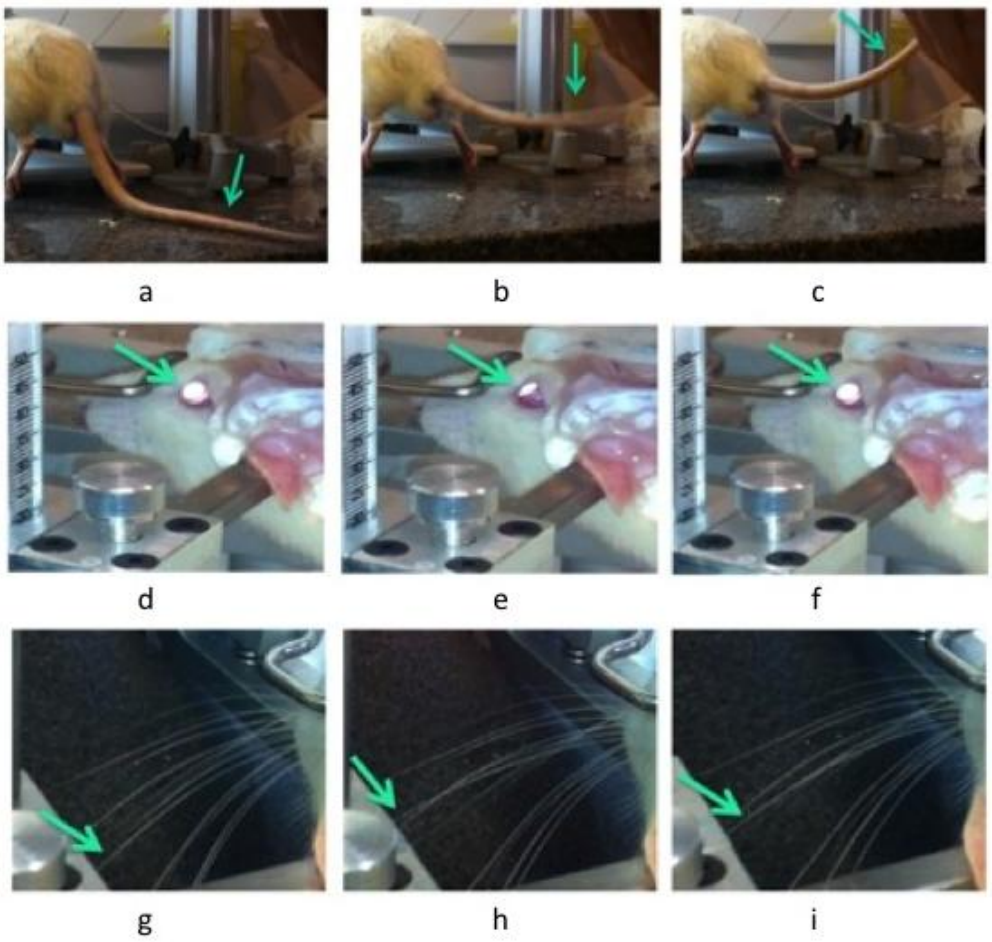

Figure 4 (a, b, c): Successive frames of motor stimulations, classified as strong motor response of the tail. a- Prior to sonication. b- Right after the ultrasound pulse. c- After the stimulation. (d, e, f): Triggered motor response of the occulomotor system of the rat .d- First frame before the ultrasound pulse. e- Frame corresponding to the ultrasound pulse – the led lights up in the foreground. f- Frame after the ultrasound pulse. (g, h, i): Triggered motor response of a single whisker of the rat .g- First frame before the ultrasound pulse. h- Frame corresponding to the ultrasound pulse – the led lights up in the background. i- Frame after the ultrasound pulse.

The motor neurostimulations of very specific structures such as the occulomotor system or a single whisker are particularly interesting, since the size of the focal spot should theoretically not allow focusing only on such small brain regions (typically the occulomotor and lateral facial *nuclei* are submillimetric). One possibility is that their stimulation thresholds became lower in some of the experimental sessions due to a specific brain activity state during the animal's sleep. Another possibility is that their activation involves the stimulations or inhibitions of several other structures that a given pressure pattern is able to trigger specifically. In order to get more insight into the spatial distribution of the ultrasound pressure field, results of numerical simulations of the ultrasound beam in a full rat head model are displayed in section 3.4.

3.3 Pressure threshold

Figure 5 presents two response curves for the same animal, but at different times in the experiment, i.e. for different anesthesia stages: the motor response is plotted as a function of estimated pressure at focus, as evaluated in water, ranging from "no

response", "muscular contraction but no limb movement" to "muscular contraction with limb movement". In those compiled results, rats of the same age and weight (200 g) were used with the same anesthesia protocol and we focused on the motor stimulation of the hindlegs and tail that were more consistently obtained.

Two experimental series are presented in figure 5 on the same animal for deep and light anesthesia stages. As described in the methods section, a sigmoid fit (red curve in figure 5) was used to find the pressure thresholds, respectively 0.79 and 0.59 MPa in those cases. On average for all of the animals, we found a pressure threshold of 0.68 MPa (N=29 series), with a standard error of 0.02 MPa. Pressures are given as if in free water, without any correction applied. The standard deviation of the threshold corresponds to 0.1 MPa which is likely due to the anesthesia conditions and timing, as illustrated in figure 5a and 5b. Indeed, in the light anesthesia stage, the threshold was always found to be lower than in the early anesthesia stage (0.59 MPa in figure 5b versus 0.79 MPa in figure 5a), while the sigmoid also appears less sharp in figure 5b, indicating more deviation in the responses for late anesthesia.

By focusing only on some of the results on which the pedal reflex was used as a classification tool between light and deep anesthesia (N=7 series), we found a threshold of 0.77 ± 0.04 MPa for early (deep) anesthesia (N=3 series, SE=0.02 MPa) and 0.61 ± 0.03 MPa for late (light) anesthesia (N=4 series, SE=0.015 MPa).

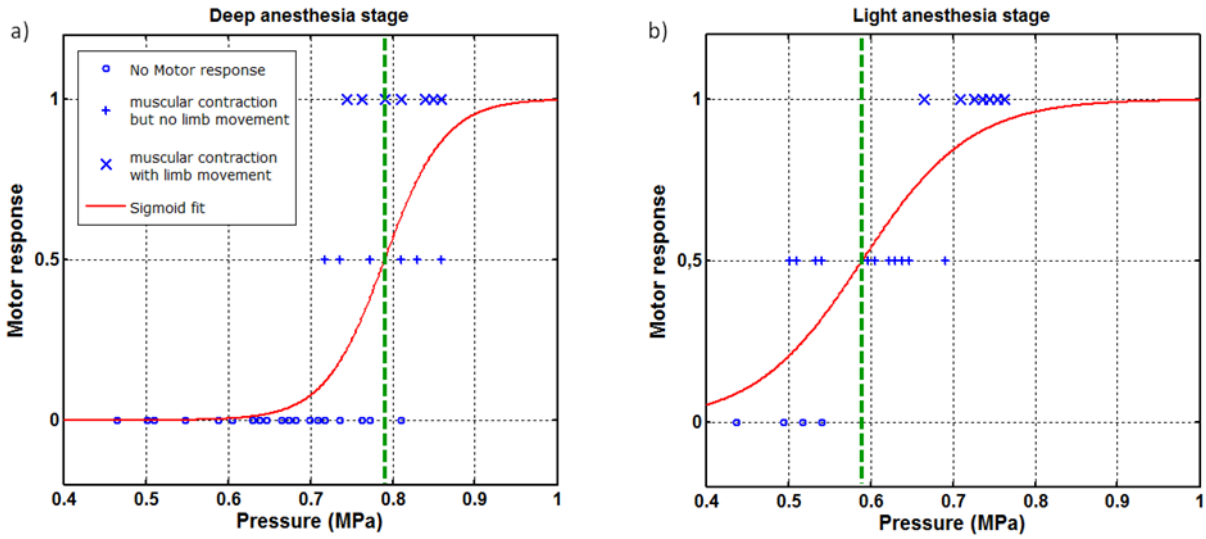

Figure 5 (a, b): Two response curves corresponding to different anesthesia stage on the same rat during the same experiment. a- In the beginning of the experiment, the sigmoid presents a sharp threshold at 0.79 MPa (uncorrected pressure). b- In the last minutes of the experiment, the sigmoid is not as sharp with a lower threshold around 0.59 MPa which corresponds to a diminishing threshold while the animal starts to wake up slowly.

All of those pressure thresholds are estimated in water for the equivalent input voltage, i.e. uncorrected for the skull transmission or any other effects. In order to provide values closer to the reality inside the brain, numerical simulations of the acoustic field in a full head model were performed and correction values for the pressure and intensity peaks are estimated in the next section.

3.4 Acoustic numerical simulation of the experiment

Numerical simulations of the acoustic field were performed using the geometry of the transducer and a CT scan of the rat head. All of the ultrasonic parameters were similar to the real experiment.

Figure 6 presents the temporal pressure profile obtained at the geometric focus for the three configurations. In the case of the full head model, the pressure is not steady and oscillates over time due to the construction of interferences in the head. It is also noticeable that the pressure is not zero, even after the end of the ultrasound pulse emission due to strong reverberations inside the head cavity, although the pressure amplitude is reduced by a factor two. This behavior is also present, albeit with a much lower pressure amplitude left, in the case of pressure curves through the half skull in water due to reverberations between the skull surface and the transducer and inside the coupling cone respectively. In the case of the half-skull, the time profile clearly shows the interferences between the direct and reflected waves which appear to be primarily destructive in the case presented below (t=120 µs…).

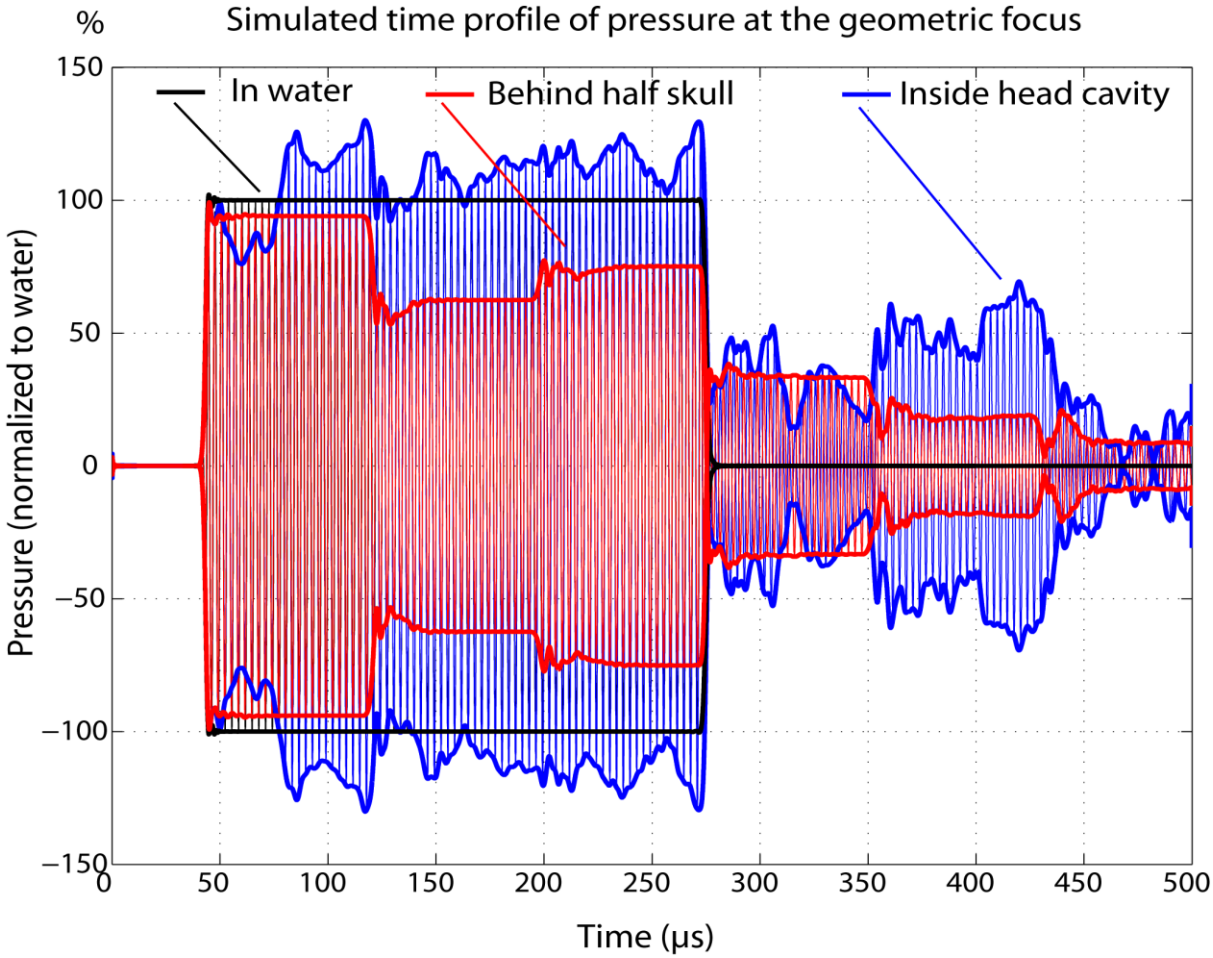

Figure 6: Simulated pressure amplitude at the geometric focus as a function of time; in free water (black), in the full head model (blue) and behind the half skull (red).

In order to quantify the overall increase in peak pressure, the spatial peak and time peak pressures were estimated for each configuration and normalized to that corresponding to the free water simulation. Peak pressure maps for the water and full head

configuration in the sagittal, coronal and horizontal planes are presented in figure 6. One can notice that the full head configuration shows considerable interference patterns with secondary and shifted peaks and an overall increased peak pressure inside the head due to standing waves. Those patterns arise in the full head and not only inside the animal brain, suggesting that the air-tissue interface is the primary cause of the reverberations in front of the tissue-skull interface, which could be expected given the small thickness of the skull with respect to wavelength.

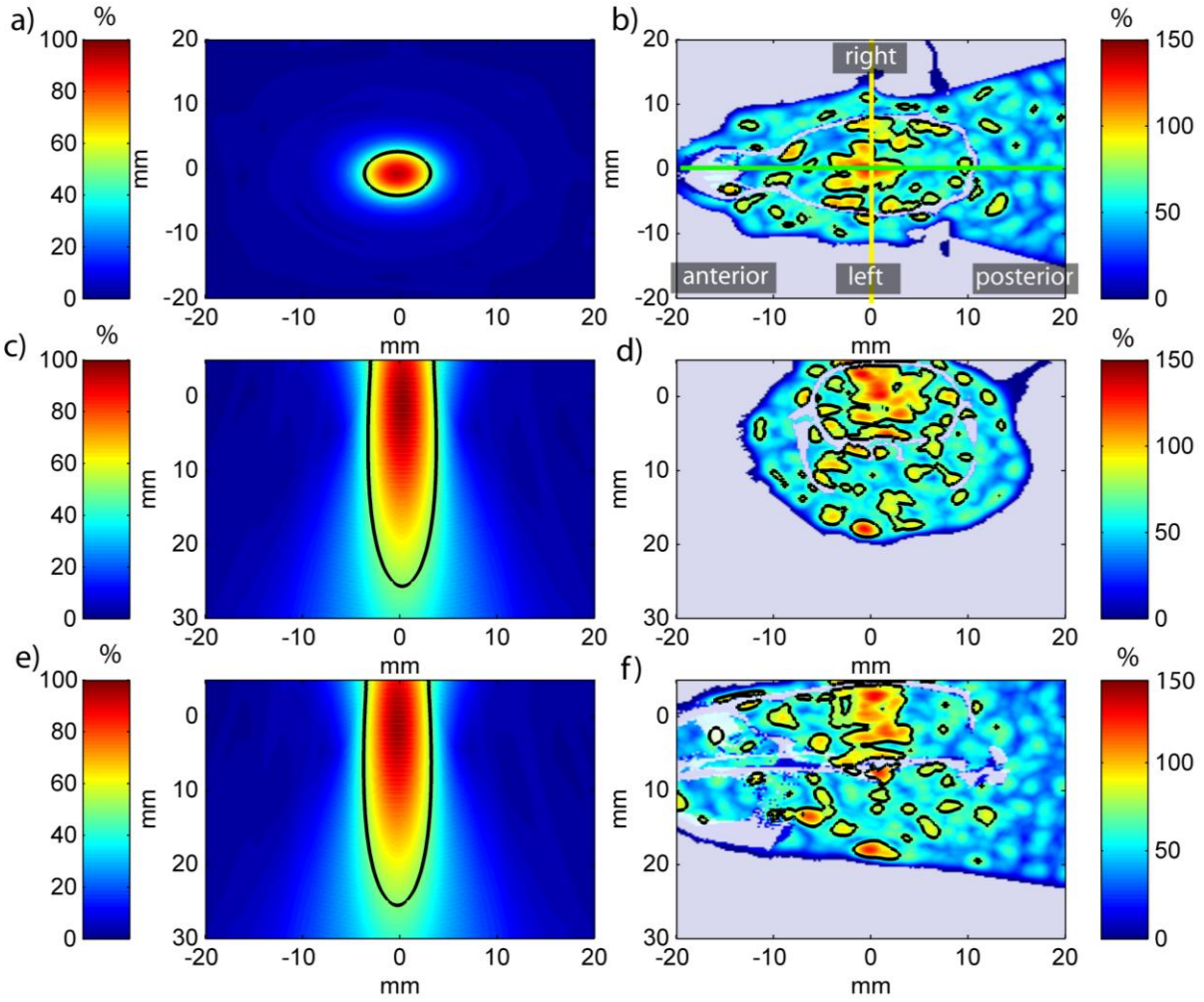

Figure 7 (a, b, c, d, e, f): Peak pressure spatial distribution relative to the peak pressure in water (%). Note the change in color-bar scale between the two columns. The isocontour represents half maximum of each configuration. a- Peak pressure map in water (horizontal view). b- Equivalent view for the full head model (skull is represented in white). c- Peak pressure map in water (coronal view). d- Equivalent view for the full head model. e- Peak pressure map in water (sagittal view). f- Equivalent view for the full head model.

Spatial profiles of the time peak pressure are given in figure 8, for the free water and full head configurations along the coronal and sagittal axes and centered at the geometric focus. It is clear that in these spatial profiles, that there is both a uniform background pressure of approximately 40% of the spatial peak, time peak pressure in water (approximately 30% of the spatial peak, time peak pressure in the brain) and multiple secondary peaks that are smaller than the focal spot in water, which are typically half-a-

wavelength wide and are expected in the case of standing wave interferences forming in a cavity.

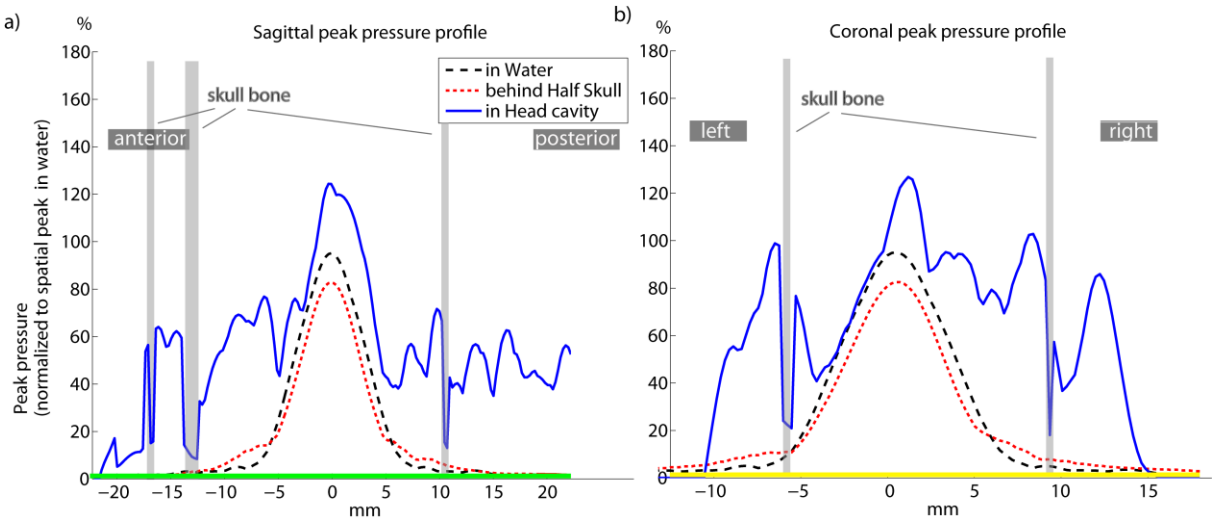

Figure 8. Spatial profiles at the geometric focus. a- Coronal axis. b- Sagittal axis. Skull bone is indicated in gray. The profiles show spatial oscillations of approximately half a wavelength typical of standing waves pattern. Although this gives rise to peaks smaller than the focus spot in water, the pressure is not well focused and is distributed over the whole head at approximately 30% of the peak value in the head cavity (40% of the peak value in free water).

As presented in Table 3, the spatial peak, time peak pressures were estimated for the half skull and full head configuration and normalized to the spatial peak, time peak pressure simulated in free water. Since part of the transmitted pressure is due to constructive or destructive interferences between the transducer and the half-skull as evidenced by the pressure profile behind the half skull in figure 6, we averaged the results over 10 different positions of the transducer when estimating the pressures and intensities.

Simulations of the experiment	Mean ± Std
Spatial peak, time peak pressure behind the half skull normalized to water	1.1 ± 0.2
Spatial peak, time peak pressure inside the head normalized to water	1.8 ± 0.4
Spatial peak, time peak intensity behind the half skull normalized to water	1.1 ± 0.2
Spatial peak, time peak intensity inside the head normalized to water	3.6 ± 1.8
Spatial peak, pulse averaged intensity behind the half skull normalized to water	0.9 ± 0.4
Spatial peak, pulse averaged intensity inside the head normalized to water	2.3 ± 1

Table 3: Simulated pressures and intensities behind the half skull and inside the head normalized to those in free water.

We estimate that the spatial peak, time peak pressure inside the head of the animal has a 1.8-fold increase, on average, due to the reverberations of the ultrasound wave. The standard deviation of this ratio due to the 10 different positions simulated was found to be 0.4 and seems mainly linked with the destructive or constructive nature of the interferences between the transducer and animal skull. The spatial peak, pulse averaged

intensity showed a 2.3-fold increase for a 3.6-fold increase for the spatial peak, time peak intensity. Intensity and pressure are thus very different from estimation based on water measurements only and could potentially lead to local tissue heating even when the acoustic intensity was initially found to be low in water (table 3).

Regarding the transmission through the half skull, we observe on the pressure time profile behind the half skull (red curve in figure 6) an initial transmission of 90%, before the interferences start to play a role either destructively or constructively. This value is close to the experimental transmission found on three skulls (cf. table 3).

4. Discussion:

This work confirms the existence of a pressure threshold in the brain for motor stimulation using transcranial focused ultrasound. The ultrasonic sequence for neurostimulation was based on that described in detail in Nature Protocols[21]. Only the pressure amplitude was modified, and all other ultrasonic parameters were kept constant. This enables the study of a single parameter in order to evaluate the existence of a neurostimulation threshold. However, it does not permit the conclusion of whether the threshold is a mechanical threshold or a thermal threshold, which remains an open question. In further studies, several different transmit sequences (changing PRF, duty cycle and pressure amplitude) should be used in order to answer this question.

Failure to obtain any motor response was observed in 40% of the attempts, even though the same protocol was followed and was specific for a given animal and a given day. It can be hypothesized that any change in the anesthetic cocktail or in the physiological state of the animal that day can play a major role in these experiments. Even though we suspect anesthesia, no correlation could be done with any specific animal, or the date of the opening of the anesthetic cocktails. When successful (60%), the experiments were consistent for the whole experimental session on a particular day and always demonstrated an acoustic threshold, as shown in Figure 5a and 5b. The mean pressure value was 0.68 ± 0.1 MPa (N series=29), given in free water. One should also notice that depending on the anesthesia stage the threshold varied from 0.61 ± 0.03 MPa (N series=3) to 0.77 ± 0.04 MPa (N series=4). The excitability thus appears to be highly dependent on the anesthesia. Those pressures are again given in free water, uncorrected for skull transmission or reverberations, and correspond to an average Isppa of 7.5 W/cm^2.

For most experiments on acoustic neurostimulation published in the literature, the acoustic pressure values and Isppa reported correspond to calibration experiments performed in free water or behind a half skull only. Our results are consistent with those observed by Yoo et al[7] on the rabbits who found a Isppa of about 12.5 W/cm^2 using limb movements and considering we used a much lower frequency (320 kHz versus 690 kHz) which is known to reduce the threshold[6,19]. Comparison with other published studies is difficult due to the different protocols involved in terms of motor threshold definition (EMG statistics versus limb movement), species, acoustic parameters or anesthesia levels[6,19].

Based on our numerical simulations, the acoustic pressure induced *in situ* was found to be strongly biased by the influence of ultrasound reverberations in the head cavity. The tissue-air interfaces were found to be predominant in generating such reverberations compared to the tissue-skull interfaces. In simulations, taking into account only the half

skull transmission does not yield a satisfying estimation of the acoustic pressure inside the animal head.

At 320 kHz, a mean 1.8-fold increase in spatial peak, time peak pressure inside the rat head compared to free space simulations was determined here. This indicates that the acoustic pressure threshold for motor threshold, which was found to be around 0.7 MPa based on free water measurement, should be corrected to approximately 1.2 ± 0.2 MPa. A 2.3-fold increase was found for the pulse-averaged intensity. This indicates that the maximum energy deposition in the brain is two times higher than expected and thermal effects could thus be higher than anticipated.

Applying these corrections on the estimation of the Mechanical index (MI) and Intensity Spatial Peak Pulse Average (Isppa) would yield a threshold of respectively MI=2.2 for the mechanical index and Isppa=17.5 $W.cm^{-2}$.

The correction of such biases should be taken into account when comparing results obtained with different frequencies, as well as the results from different species with significantly different head size, since, in both cases, the reverberations should be highly dependent on those parameters.

Moreover, the spatial distribution of pressure field using the 320 kHz ultrasound transducer was found to be strongly spread over the entire brain with much of the brain still receiving approximately 30% of the peak pressure *in situ*. Moreover, many secondary peaks were found, with a size of half a wavelength smaller than the focal spot in free water and typical for interferences pattern.

Even though the locations of those secondary peaks were not linked to any specific structure on a brain atlas, such random sub-wavelength peaks could provide new insight into the fine activations sometimes observed, such as for a single whisker or eye movement, which involve very small brain structures. It cannot be excluded, however, that these specific activations are simply the results of lower activation thresholds in the corresponding structures due the anesthesia level or to the brain activity state.

Those results tend to show that the neurostimulating acoustic field is much more complex than a single localized acoustic spot at the geometric focus. Combined with the intrinsic variability and complexity of the brain activity and its dependence on the anesthesia level and sleep state, it might be difficult to assess the mechanisms behind neurostimulation in such configurations. Simpler configurations that are less prone to reverberations, such as shorter pulse, higher frequencies, or chirps[26, 20, 29], or simply larger animals could help in further simplifying the acoustic problem and looking at the neurostimulation effect itself. For a given frequency, such reverberation effects and pressure field distortion should be much lower in primate or human heads due to the larger size of the head. Additional numerical and experimental studies[26] will be required to quantify this effect when investigating motor thresholds and safety in those species.

5. Conclusion:

A transient motor response has been elicited in anesthetized rats by 320 kHz transcranial ultrasound in more than 60% of the experimental sessions, with a pressure threshold estimated at 0.68 MPa (Isppa= 7.5 $W.cm^{-2}$, Mechanical Index=1.2) as measured in free water. In some cases, the stimulation of very specific structures such as the occulomotor system or a single whisker was observed, even though the wavelength at 320 kHz is approximately 5 mm. Simulation using a finite-difference-time-domain

software and CT scan shown ultrasound reverberations in the head cavity yielding a 1.8-fold increase of the spatial peak, time peak pressure compared to free water and a 2.3-fold increase of spatial peak, pulse averaged intensity. At this low frequency, several sub-wavelength peaks are also created. The acoustic field resulting from the reverberations needs to be carefully taken into account for small animal studies at low frequencies.

Bibliography

[1] J. Kennedy, "High-intensity focused ultrasound in the treatment of solid tumors," Nat. Rev. Cancer (2005).

[2] M. Pearle, "Shock-Wave Lithotripsy for Renal Calculi," New Engl. J. Med. (2012).

[3] F. Fry, H.W. Ades, and W.J. Fry, "Production of reversible changes in the central nervous system by ultrasound," Science **127**(3289), 83–4, (1958).

[4] E.E. Gavrilov L R, Gersuni G V, Ilyinsky O B, Sirotyuk M G, Tsirulnikov E M, Shchekanov, "The effect of focused ultrasound on the skin and deep nerve structures of man and animal," Prog. Brain Res. **43**, 279–92, (1976).

[5] W.J. Tyler, Y. Tufail, M. Finsterwald, M.L. Tauchmann, E.J. Olson, and C. Majestic, "Remote excitation of neuronal circuits using low-intensity, low-frequency ultrasound," PloS One **3**(10), e3511, (2008).

[6] Y. Tufail *et al.*, "Transcranial pulsed ultrasound stimulates intact brain circuits," Neuron **66**(5), 681–94, (2010).

[7] S.-S. Yoo *et al.*, "Focused ultrasound modulates region-specific brain activity," NeuroImage **56**(3), 1267–75, (2011).

[8] J.-L. Thomas and M.A. Fink, "Ultrasonic beam focusing through tissue inhomogeneities with a time reversal mirror: application to trans-skull therapy," IEEE Trans. Ultrason. Ferroelect. Freq. Control **43**(6), 1122–1129, (1996).

[9] M. Tanter, J.-L. Thomas, and M. Fink, "Focusing and steering through absorbing and aberrating layers: Application to ultrasonic propagation through the skull," J. Acoust. Soc. Am. **103**(5), 2403, (1998).

[10] K. Hynynen and J. Sun, "Trans-skull ultrasound therapy: the feasibility of using image-derived skull thickness information to correct the phase distortion," IEEE Trans. Ultrason. Ferroelect. Freq. Control **46**(3), 752–5, (1999).

[11] M.A. Nitsche *et al.*, "Transcranial direct current stimulation: State of the art 2008," Brain Stimul. **1**(3), 206–23, (2008).

[12] K.J. Ressler and H.S. Mayberg, "Targeting abnormal neural circuits in mood and anxiety disorders: from the laboratory to the clinic," Nature Neurosci. **10**(9), 1116–24, (2007).

[13] M. Hallett, "Transcranial magnetic stimulation and the human brain," Nature **406**(6792), 147–50, (2000).

[14] S. Szobota *et al.*, "Remote control of neuronal activity with a light-gated glutamate receptor," Neuron **54**(4), 535–45, (2007).

[15] F. Zhang, A.M. Aravanis, A. Adamantidis, L. de Lecea, and K. Deisseroth, "Circuit-breakers: optical technologies for probing neural signals and systems," Nature Rev. Neurosci. **8**(8), 577–81, (2007).

[16] P.S. Yang *et al.*, "Transcranial focused ultrasound to the thalamus is associated with reduced extracellular GABA levels in rats," Neuropsychobiol. **65**(3), 153–160, (2012).

[17] M.J. Borrelli, K.I. Bailey, and F. Dunn, "Early ultrasonic effects upon mammalian CNS structures (chemical synapses)," J. Acoustic Soc. Am. **69**(5), 1514–6, (1981).

[18] B. Krasovitski, V. Frenkel, S. Shoham, and E. Kimmel, "Intramembrane cavitation as a unifying mechanism for ultrasound-induced bioeffects," PNAS **108**(8), 3258, (2011).

[19] R.L. King, J.R. Brown, W.T. Newsome, and K.B. Pauly, "Effective parameters for ultrasound-induced in vivo neurostimulation," Ultrasound Med. Biol. **39**(2), 312–31, (2013).

[20] M. a O'Reilly, Y. Huang, and K. Hynynen, "The impact of standing wave effects on transcranial focused ultrasound disruption of the blood-brain barrier in a rat model," Phys. Med. Biol. **55**(18), 5251–67, (2010).

[21] Y. Tufail, A. Yoshihiro, S. Pati, M.M. Li, and W.J. Tyler, "Ultrasonic neuromodulation by brain stimulation with transcranial ultrasound," Nature Protocols **6**(9), 1453–1470, (2011).

[22] D. Royer, N. Dubois, and M. Fink, "Optical probing of pulsed, focused ultrasonic fields using a heterodyne interferometer," Appl. Phys. Letters **61**(2), 153, (1992).

[23] J.-F. Aubry, M. Tanter, M. Pernot, J.-L. Thomas, and M. Fink, "Experimental demonstration of noninvasive transskull adaptive focusing based on prior computed tomography scans," J. Acoustic. Soc. Am. **113**(1), 84, (2003).

[24] M. Tanter, M. Pernot, J.F. Aubry, G. Montaldo, F. Marquet, and M. Fink, "Compensating for bone interfaces and respiratory motion in high-intensity focused ultrasound," Intl. J. Hyperthermia **23**(2), 141–51, (2007).

[25] F. Marquet *et al.*, "Non-invasive transcranial ultrasound therapy based on a 3D CT scan: protocol validation and in vitro results," Phys. Med. Biol. **54**, 2597, (2009).

[26] T. Deffieux and E.E. Konofagou, "Numerical study of a simple transcranial focused ultrasound system applied to blood-brain barrier opening," IEEE Transact. Ultrason. Ferroelect. Freq. Control **57**(12), 2637–53, (2010).

[27] International Commission on Radiation Units and Measurements, *ICRU Report 61: Tissue Substitutes, Phantoms and Computational Modeling in Medical Ultrasound* (Bethesda, MarylandICRU Publications, 1998).

[28] M.O. Culjat, D. Goldenberg, P. Tewari, and R.S. Singh, "A review of tissue substitutes for ultrasound imaging," Ultrasound Med. Biol. **36**(6), 861–73, (2010).

[29] S.C. Tang and G.T. Clement, "Standing-wave suppression for transcranial ultrasound by random modulation," IEEE Transact. Biomed. Eng. **57**(1), 203–5, (2010).